Title: Frogs uncouple neural activity from oxygen consumption after hibernation

Authors: Hafsa Yaseen[1], Joseph M. Santin[1*]

Affiliations: [1]University of Missouri-Columbia, Division of Biological Sciences, Missouri, United States of America.

***Email for correspondence**: santinj@missouri.edu

Funding statement: This work was supported by the following grants: National Science Foundation-Award # 2515635 (to JMS) and National Institutes of Health- R01NS114514 (to JMS).

Conflict of interest disclosure: The authors do have conflicts of interest to declare.

Ethics approval statement: Approval for the use of animals was approved by the Animal Care and Use Committee at the University of Missouri (protocol #39264).

Abstract

Brain activity is costly, and aerobic metabolism supplies ~90% of the ATP for cellular and synaptic function. Accordingly, oxygen consumption varies to match activity demands of neural circuits, and mitochondrial defects that reduce aerobic metabolism cause various neurological disorders. Brain activity in frogs has energy demands typical of an average vertebrate, but surprisingly, improves function upon stopping oxidative metabolism from a few minutes to hours following hibernation. While this represents a large capacity to shift to glycolysis as a lone ATP source in an adult brain circuit, we hypothesized activity's reliance on oxygen may be globally reduced. We tested this by simultaneously assessing tissue oxygen consumption and neural activity from a brainstem motor network. We show that hibernation triggers a reduction in the oxygen consumed by neural activity and activity-independent mitochondrial respiration. In accordance with lower aerobic requirements, network output remained stable over a wide range of tissue oxygen levels, from baseline to anoxia, whereas controls were disrupted by moderate hypoxia. Despite operating with reduced aerobic metabolism, network activity was similar to controls, and activity increases did not accelerate oxygen consumption until seizure-like bursts ensued. Therefore, circuits in the vertebrate brain have the surprising capacity to uphold normal network functions with reduced aerobic metabolism. These findings introduce low-cost states can lie dormant within otherwise energetically expensive circuits and raise the question why costly designs are the default when they, in some cases, may be unnecessary and predispose organisms to metabolic pathologies.

INTRODUCTION

Brain function is energetically expensive[1,2]. At the circuit level, synaptic transmission and the restoration of ion gradients following action potentials have high ATP demands, the majority of which is supplied by oxidative phosphorylation in mitochondria[3,4]. Given the ATP yield of aerobic respiration (30-32 moles ATP/1 mole glucose) compared to glycolysis (2 moles of ATP/1 mole of glucose), neural activity and oxygen consumption are tightly coupled, whereby increases in activity drive aerobic metabolism to sustain neuronal performance[5–7]. This relationship is especially critical, as disruptions to ATP synthesis within the mitochondrial impair neural output and lead to neurological disease[8]. The requirement for aerobic respiration is conserved across phyla and has shaped prevailing views that sustained neural computation requires oxygen consumption[9].

Despite the view that neural activity's large energy demands remain fixed, the American bullfrog (*Aquarana catesbeiana*) provides a unique opportunity to address how neural circuits can enter states that operate with far less energy. Under normal circumstances frog circuits exhibit typical metabolic demands and rely heavily on oxidative metabolism[10,11]. However, activity of brainstem motor circuits that generate breathing improve function during anoxia from ~10 minutes to upwards of 4 hours under otherwise identical experimental conditions after frogs emerge from hibernation[12,13]. This represents a striking display of metabolic plasticity, as this network has high metabolic demands, with rhythm generating circuits that use glutamatergic synaptic transmission, which is thought to incur large energy costs, and motor pools with neurons that fire action potentials at rates >100 Hz during rhythmic bursting[14–16]. Mechanistically, there are two non-mutually exclusive possibilities that could explain how hibernation drives this response: increasing ATP supply during hypoxia and/or reducing the metabolic cost of activity. First, while glycolysis produces ~15-fold less ATP than oxidative phosphorylation, hypoxia can increase glycolysis through the Pasteur effect. Thus, hibernation may lead to cellular changes that bolster flux through glycolysis[17] to sustain neural activity without oxygen. On the other hand, hibernation may reduce the cost of neural activity such that similar network output is generated with less energy. While there are several ways

31 neuronal circuits could in principle alter their energy efficiency[18–20], hibernation reduces
32 the Ca^{2+} permeability of NMDA-glutamate receptors and enhances receptor
33 desensitization[21], which is likely to reduce the energetic burden of ion regulation at
34 synapses. Resolving these possibilities may provide new insight into the evolutionary
35 pressures that govern metabolic constraints on neural circuits, as well as lead new ideas
36 for how to protect the mammalian brain against dysfunction of metabolic origin.

37 In this study, we assessed the extent to which hibernation alters activity's energetic
38 requirements in the brainstem respiratory network. To estimate the aerobic metabolic cost
39 of activity under normal (control) and hypoxia-tolerant (after hibernation) network states,
40 we simultaneously measured network activity through motor nerve rootlets and tissue
41 oxygen partial pressure (pO_2) within the rhythm-generating circuit *in vitro*. This approach
42 allows us to estimate aerobic metabolism because tissue pO_2 reflects consumption by
43 mitochondria without the confound of cerebral blood flow, where pO_2 decreases relate to
44 greater rates of aerobic metabolism and increases reflect less oxygen consumption[5,22].
45 We then assessed which cellular processes alter their energy requirements, the
46 relationship between tissue pO_2 and activity, and how oxygen consumption varies over a
47 range of network intensities. Collectively, results here indicate that hibernation uncouples
48 physiological activity from its typical aerobic requirement, demonstrating that the same
49 neural circuit within a single species can enter states that require less aerobic respiration
50 while upholding physiological function.

51

METHODS

Experimental model

All procedures were approved by the Animal Care and Use Committee at the University of Missouri (protocol #39264). Adult female American bullfrogs (*Aquarana catesbeiana*, ~100 g; n = 51) were obtained from Rana Ranch (Twin Falls, ID, USA) and housed in 20-gallon tanks containing dechlorinated, aerated water at room temperature on a 12-h light/dark cycle. Frogs had access to wet and dry platforms, were fed weekly, along with daily water checks and weekly water changes. Control animals were acclimated for ≥1 week before experiments. A subset of frogs was subjected to a simulated hibernation protocol. Food was withheld and water temperature was decreased from room temperature to 4°C over 10 days in a temperature-controlled chamber. Once at 4°C, air access was blocked using a perforated screen to enforce continuous submergence, and frogs were maintained for 4 weeks before experimentation. Frogs subjected to the cold-submergence treatment are referred to here as "hibernators," following prior work showing that similar protocols induces metabolic suppression, consistent with the definitions of hibernation that involve reduced whole-animal metabolism beyond that which is driven by reduced temperature alone[23].

Brainstem–Spinal Cord Preparation

Brainstem–spinal cord preparations were obtained as described previously[24]. Frogs were anesthetized with isoflurane (~1 ml/L; v/v) until the toe-pinch reflex was no longer present, then rapidly decapitated with a guillotine. The head was submerged in ice-cold bullfrog artificial cerebrospinal fluid (aCSF; in mM: 104 NaCl, 4 KCl, 1.4 $MgCl_2$, 7.5 glucose, 40 $NaHCO_3$, 2.5 $CaCl_2$, and 1 NaH_2PO_4; bubbled with 98.5% O_2/ 1.5% CO_2; pH 7.85). The forebrain was removed, and the brainstem–spinal cord preparation (including the midbrain, brainstem, cut caudal to the hypoglossal nerve roots) was isolated with nerve roots intact and transferred to a recording chamber continuously superfused with oxygenated aCSF. Chamber temperature was maintained at 22°C using a Warner Instruments CL-100 bipolar temperature controller with the thermistor placed adjacent to the tissue. Motor output was recorded from the vagus nerve (cranial nerve X) using glass suction electrodes. Signals were AC-amplified (1000×, Model 1700; A-M Systems,

82 Carlsborg, WA), filtered (10Hz-5kHz), digitized (PowerLab 8/35, ADInstruments,
83 Colorado Springs, CO), rectified, and integrated online (time constant = 100 ms) to
84 visualize rhythmic motor bursts. Vagus nerve output was allowed to stabilize for ≥1h in
85 aCSF bubbled with 98% O_2/1.5% CO_2 prior to any experimental manipulation.

86 **Oxygen Profiling**

87 Tissue oxygen partial pressure (pO_2) was measured using a Clark-type microsensor (OX-
88 50; Unisense A/S, Denmark) with a 50 μm tip diameter, defining a local detection volume
89 on the order of tens of microns. The sensor has a response time of ~5 s, resulting in a
90 ~5s temporal averaging of the pO_2 signal with a negligible oxygen consumption relative
91 to tissue, drawing $4x10^{-4}$-5×10^{-3} nmol O_2/hr during operation. The sensor was calibrated
92 at 22 °C in air-saturated water and in an anoxic solution (0.1 M sodium ascorbate in 0.1
93 M NaOH). The analog signal from a PA2000 amplifier (Unisense A/S) was digitized
94 through an ADC-216USB converter. For all experiments, the sensor was inserted slightly
95 lateral to the midline of the brainstem in between the vagus and trigeminal nerves. The
96 tissue pO_2 was recorded in 50 μm vertical steps from the surface to a depth of 350 μm,
97 an area that encompasses part of the respiratory network[25]. At each 50 μm vertical step,
98 the sensor was allowed to stabilize for 20 seconds before recording the pO_2 value, which
99 was taken as the tissue pO_2 at that depth. In 6 experiments for each group, the sensor
100 was advanced 650 μm, near the center of the tissue.

101

102 The amphibian respiratory network tends to produce rhythmic output with bursts often
103 clustered into stronger multi-breath episodes but can also assume a variety of output
104 patterns[26]. While the respiratory network is distributed throughout the brainstem[25], tissue
105 pO_2 fluctuations detected by the microsensor typically occurred in phase with "crescendo-
106 like" breathing episodes when these occurred (Figure 1A), confirming that the sensor
107 reported oxygen dynamics within or around the region of the active respiratory network.
108 The sensor was only able to detect oxygen fluctuations associated with these high-drive
109 episodes that spanned the 5 s detection duration of the sensor, as individual, single bursts
110 that are most dominant in this preparation are 1s in duration, and therefore, likely produce
111 oxygen transients that are faster than the response time of the sensor. Because the

112 oxygen microsensor reports pO_2 from spatially limited region around the tip, we also
113 cannot assign the precise anatomical compartment neurons contributing to each
114 measurement (*e.g.*, in regions densely packed with cell bodies, synapses, or a
115 combination of the two). The electrode tip may lie closer to somatic regions, axon fiber
116 tracts, or synaptically dense neuropil, all of which have the potential for different degrees
117 of oxygen consumption[27]. Thus, the recorded pO_2 reflects the integrated activity of
118 multiple cellular processes within that microenvironment, which was recorded as
119 consistently as possible in the same location across experiments. Targeted assessments
120 of oxygen consumption in sub-cellular compartments require further investigation.

121 **Pharmacological Experiments**

122 To isolate which processes consume O_2 in the region of the microsensor, inhibitors
123 specific to different physiological processes that might rely on aerobic metabolism were
124 sequentially blocked while monitoring tissue pO_2 at a fixed electrode depth (350 μm). We
125 interpreted the resulting increase (or lack of response) in tissue pO_2 following the inhibitor
126 as an index of the oxygen being consumed by the targeted pathway. Thus, ΔpO_2 (the
127 steady-state O_2 reading before the application of the drug subtracted from the steady-
128 state reading after the drug) served as a functional readout of the relative metabolic
129 contribution of the process inhibited. The following final bath concentrations were applied
130 in sequence: Tetrodotoxin (TTX, voltage-gated Na^+ channel blocker, 500nM); DNQX
131 (AMPA receptor antagonist, 10μM); APV (NMDA receptor antagonist, 50μM); Bafilomycin
132 A1 (V-ATPase inhibitor, 1μM); Ouabain (Na^+/K^+-ATPase pump inhibitor, 500μM); Sodium
133 cyanide (mitochondrial Complex IV inhibitor, 5mM). Each drug was superfused until a
134 stable plateau in pO_2 was achieved (~15–20 min), and then the next was applied. Seven
135 control and seven hibernated brainstems were used. Although our pharmacological
136 approach isolates specific pathways powered by aerobic metabolism, the relative
137 magnitude of their pO_2 changes depends on their local abundance within the sampled
138 volume. As a result, oxygen consumption associated with spontaneous synaptic
139 transmission or vesicle recycling may be underestimated if the sensor was positioned
140 nearer to neuronal cell bodies than to synapse-rich zones[27]. These factors are inherent
141 to single-point oxygen microsensors and reflect the spatial averaging of pO_2 over the

142 sensor's diffusion field and require further assessments targeting specific sub-cellular
143 recordings.

144 **Graded Hypoxia and Increased Activity**

145 Graded hypoxia was induced by progressively replacing O_2 with N_2 in the aCSF using a
146 mass-flow controller (MFC-4, Sable Systems International). The N_2 fraction was
147 increased by 10% every 10 min until anoxia (0% O_2 in the reservoir) was reached. When
148 bubbled with 98.5% N_2/ 1.5% CO_2, bath pO_2 surrounding the tissue was ~15 mmHg due
149 to mixing at the liquid-air interface. In all controls and hibernators, tissue pO_2 at the sensor
150 reported 0 mmHg; thus, we refer this outcome as "anoxia." However, the detection limit
151 for the OX-50 sensor is ~0.3 μmol/L (~0.165 mmHg under our experimental conditions;
152 22°C, ~755 mmHg atmospheric pressure). Therefore, while the sensor reported 0 mmHg
153 inside the tissue when bathed with solution gased with 98.5% N_2/ 1.5% CO_2 (and in some
154 cases at even higher fractions of O_2), it is not possible to resolve differences in tissue pO_2
155 between 0- 0.165 mmHg. Regardless, a zero reading under these conditions reflects an
156 infinitesimal amount of O_2 should any exist in the tissue. Six control and six hibernated
157 brainstems were tested in this series. Tissue pO_2 and respiratory burst frequency were
158 recorded continuously (n = 6 controls; n = 6 hibernators). We interpret p_{crit} as the O_2
159 tension where oxidative phosphorylation decreases to a point that can no longer preserve
160 normal neural activity, beyond which activity was either chaotic or intermittent.

161

162 To assess the metabolic cost of elevated physiological activity, isoproterenol (10 μM) was
163 bath-applied after ≥1 h of stable baseline activity and superfused for 30min (n=7 controls;
164 n=6 hibernators). While other stimuli such as hypercapnia could be used to stimulate
165 respiratory frequency, in our hands, the responses can be inconsistent from preparation
166 to preparation, while isoproterenol produces consistent increases in frequency. To
167 evaluate responses to pathological hyperexcitability, bicuculline methiodide (10 μM) was
168 superfused for 30 min to induce non-respiratory, seizure-like bursts (n=6 per group). Non-
169 respiratory bursts were manually counted based on their prolonged duration and distinct
170 waveform morphology, as previously described[28]. The oxygen microsensor integrates
171 over ~5s which does not resolve the rapid pO_2 transients associated with individual

respiratory bursts (~1s duration). Therefore, pO_2 data for these experiments reflect longer-timescale changes in tissue oxygen dynamics, rather than instantaneous fluctuations tied to single bursts. This averaging is appropriate for quantifying sustained differences in oxygen consumption over minutes, which were apparent in these experiments.

Drugs

Tetrodotoxin (TTX), DNQX, APV, and bicuculline were obtained from Hello Bio. Bafilomycin A1 was purchased from Cayman Chemical. Ouabain was obtained from Thermo Scientific, sodium cyanide from MP Biomedicals, and isoproterenol from Tokyo Chemical Industry. All drugs were prepared as stock solutions according to manufacturer recommendations and diluted to final concentrations in artificial cerebrospinal fluid immediately prior to use.

Data Analysis

Respiratory burst frequency was determined from rectified and integrated vagus recordings using the Peak Analysis function in LabChart 8 (ADInstruments). Bursts were identified by standard criteria (~1 s duration) with start/stop thresholds at 5% of peak height[29]. For graded hypoxia experiments, mean burst frequency and tissue pO_2 were calculated for every 10 mmHg drop in tissue pO_2 relative to baseline at 98% O_2. For experiments involving sequential drug exposures, mean pO_2 values were obtained over the final 10 min of each treatment at steady-state. During the application of isoproterenol, pO_2 values were taken at baseline and then at 10 minute intervals sampling for 2 minutes during the 30 minute exposure. For bicuculine, pO_2 values were taken at baseline, at the trough of the large dip caused by the large non-respiratory burst following bicuculine, and then the last 5 minutes of the 30 minute exposure

Statistical analysis

Data are presented as mean ± SD or box and whisker plots unless otherwise stated. Statistical comparisons were performed in GraphPad Prism v10.6.1 (San Diego, CA, USA). Two-way repeated measures ANOVA was applied with two independent variables and one dependent variable (e.g., the effect of depth and group on tissue pO_2). In these

cases, Holm–Šidák multiple comparisons test was applied after if there were any interaction or group effects. To assess the effects of tissue pO_2 and burst frequency, we used a mixed linear model with restricted maximum likelihood, as this dataset had many missing values due to the differing starting points of pO_2 from preparation to preparation. Unpaired t tests were used to compare two independent groups. Individual data points are shown where appropriate to show variability among preparations.

207 **RESULTS**

208 The amphibian respiratory network *in vitro* generates output that occurs as
209 rhythmic bursts, which are periodically interrupted by high-drive breathing events termed
210 episodes[30]. While the electrochemical sensor used in this study could not resolve O_2
211 changes associated with single bursts which last ~1s, when breathing episodes spanned
212 several seconds, pO_2 transients of a few mmHg occurred in phase (Figure 1A). This
213 supporting the detection of oxygen consumption within or around the active respiratory
214 network. Despite having similar baseline network outputs (Figure 1B), hibernators had
215 higher average tissue pO_2 across the range of depths from the surface of the brainstem
216 to 350 µm at the baseline external O_2 levels (Figure 1C), and also in 6 additional
217 preparations that were measured down to 650 µm near the center of the tissue
218 (Supplemental Figure 1). Moreover, lowering the oxygen in the bathing solution
219 decreased tissue pO_2 as expected, but values were higher in hibernators at most fixed
220 external pO_2 (Figure 1D). These observations indicate a reduction in brainstem O_2
221 consumption in hibernators when oxygen is present.

222 We then used a pharmacological approach to identify which of the ATP-consuming
223 processes use less oxygen. For this, we measured changes in averaged tissue pO_2 during
224 the sequential application of inhibitors (Supplemental Figure 2) that block network activity
225 (tetrodotoxin; TTX), action potential-independent spontaneous excitatory postsynaptic
226 potentials (DNQX and APV), the synaptic vesicular ATPase (bafilomycin), the Na^+-K^+
227 ATPase that maintains resting ion gradients (ouabain), and complex IV of the
228 mitochondrial respiratory chain (sodium cyanide), each of which has the potential to
229 represent energy sinks in the brain[20,31] (Figure 1E). In controls, TTX increased tissue pO_2,
230 demonstrating the consumption of oxygen to power baseline activity. Blocking
231 spontaneous excitatory transmission and then the V-ATPase had no further effects on
232 tissue pO_2. Inhibition of the Na^+-K^+ ATPase then raised tissue pO_2, demonstrating a
233 metabolic cost of regulating resting Na^+ and K^+ gradients. Poisoning mitochondria with
234 cyanide to inhibit remaining background respiratory activity led to a large increase in
235 tissue pO_2. When performing the same protocol on hibernators, less O_2 was consumed
236 by activity compared to controls, as TTX led to a smaller rise in tissue pO_2. The other

237 activity-independent processes consumed similar amounts of O_2 as controls. However,
238 hibernators showed a significantly smaller pO_2 increase upon blocking mitochondrial
239 Complex IV with sodium cyanide, suggesting a reduction in basal mitochondrial oxygen
240 consumption (Figure 1F). These results indicate that reduced oxygen consumption in
241 hibernators is driven primarily by decreasing the cost of network activity and activity-
242 independent mitochondrial respiration.

243 Since hibernators had a reduced reliance on aerobic metabolism, we predicted
244 that activity would be less sensitive to oxygen reductions and the associated decrease in
245 aerobic metabolism. In control brainstems (n = 6), network activity decreased with tissue
246 pO_2 during graded reduction in bath O_2. Each control preparation reached a critical tissue
247 pO_2 (p_{crit}), beyond which the output either lost its rhythmicity or assumed a slow disrupted
248 pattern of output while decreasing in average frequency (Figure 2A). In contrast,
249 hibernators maintained normal activity throughout the entire range of graded hypoxia
250 even at 0 mmHg (Figure 2B & 2C) and no apparent p_{crit} (Figure 2D). These results indicate
251 that decreasing the reliance on aerobic metabolism allows hibernators to generate normal
252 network activity across a wide range of tissue oxygen levels, from supraphysiological to
253 anoxia.

254 Beyond baseline activity, increased network activity drives oxygen consumption
255 through synaptic vesicle cycling and restoration of ion gradients for action potentials and
256 synaptic transmission, which is needed to sustain activity[3,7]. To test whether increased
257 network activity would accelerate aerobic metabolism, we bath-applied the β-adrenergic
258 receptor agonist, isoproterenol[32]. Example traces show that increases in activity were
259 associated with a significant decline in average tissue pO_2 in controls over the 30-minute
260 application, indicating increased oxygen consumption to meet the demands of elevated
261 activity (Figure 3A). In contrast, hibernators maintained a stable tissue pO_2 despite
262 achieving comparable increases in burst frequency (Figures 3B-3E). These results further
263 support that metabolic adaptation in hibernators decouples neural activity from its typical
264 aerobic support, allowing them to increase motor output without accelerating oxygen
265 consumption.

266 Finally, we asked if this metabolic decoupling extends to extreme hyperexcitability.
267 We induced pathological network activity by blocking fast GABAergic inhibition with
268 bicuculline, previously shown to generate high-amplitude bursts that resemble seizure-
269 like activity in controls and hibernators[28]. In controls, bicuculline triggered abnormal bursts,
270 which were accompanied by a large drop in tissue pO_2, indicating substantial increases
271 in aerobic respiration (Figures 4A, 4C-4D). Hibernators also exhibited an initial, large drop
272 in pO_2 following the first abnormal burst, demonstrating the ability to increase aerobic
273 metabolism when activity goes beyond the physiological range (Figures 4B-4D). While
274 the absolute decrease in pO_2 from baseline was the same in controls (Δ92 ± 36.4 mmHg)
275 and hibernators (Δ120 ± 22.4 mmHg; unpaired t-test, $p = 0.31$), after this initial
276 consumption event, hibernators stabilized at a tissue pO_2 approximately double that of
277 controls (Figures 4B and 4C), indicating that aerobic metabolism was less under the same
278 conditions. Despite less oxygen consumption in the presence of bicuculine, hibernators
279 maintained normal respiratory network output, while controls produced mainly seizure-
280 like bursts (Figure 4A inset iii, 4D). Therefore, when pushed to the extreme, hibernators
281 meet these demands by consuming O_2 but ultimately maintain activity homeostasis during
282 conditions of severe hyperexcitability with less aerobic metabolism.

DISCUSSION

Owing to the high ATP yield of aerobic respiration, increases in oxidative metabolism are thought to be essential for meeting the energy costs incurred by neural activity, from flies to mammals[6,33]. Energy limitations in neurological disorders have prompted interest in animal adaptations as sources of novel mechanisms for improving metabolic robustness in neural systems[34–38]. In frogs, hibernation transforms brainstem circuits to function during lack of oxygen by altering synapses such that glycolysis supports activity as a lone ATP source[12,13]. While impressive, we now show that neural activity can be uncoupled from its support by aerobic metabolism, even when oxygen is readily available. These results introduce that circuits with a seemingly obligate requirement for aerobic metabolism can enter a low-cost state that achieves the same functional output over a wide range of energetic challenges, including hypoxia, elevated activity, and pathological hyperexcitability, all while consuming less O_2.

Based on the cellular processes addressed, neural activity, activity-independent Na^+/K^+ ATPase turnover, and activity-independent mitochondrial respiration are main contributors of O_2 consumption in the brainstem, with minimal input from spontaneous excitatory postsynaptic currents and the V-ATPase involved in filling vesicles with neurotransmitter (Figure 1F, Supplemental Figure 2). Hibernator brainstems exhibited a reduction in O_2 consumption, driven by lower cost of activity and less activity-independent respiration. While our results implicate activity, they do not allow us to address which aspects of network activity decrease energetic needs. Synaptic transmission incurs a greater metabolic cost than action potentials in active networks[39,40], positioning them as a critical site for reducing energy consumption. Indeed, NMDA-glutamate receptors, which are involved in generating respiratory motor bursts, maintain normal postsynaptic current amplitude after hibernation but adopt a receptor profile that is less permeable to calcium and strongly desensitize, suggesting a lower cost of ion regulation[21]. We also observed an apparent reduction in the O_2 consumed by activity-independent mitochondrial respiration, which was the largest contributor to baseline O_2 consumption in both groups. This may reflect tighter coupling between electron transport and ATP synthesis due to decreased proton leak across the inner membrane, potentially driven by

313 altered uncoupling protein function, membrane lipid composition, or cristae structure that
314 enhance oxidative phosphorylation efficiency[41–45]. While we did not measure ATP
315 production directly, this interpretation implies that activity-independent ATP production
316 could be similar if less O_2 consumption was spent opposing proton leak. However, it is
317 also possible that a reduction in background O_2 consumption translates to less activity-
318 independent ATP production. While the functional implications remain to be determined,
319 less ATP production for activity-independent processes, such as lipid turnover and other
320 housekeeping functions[22,46], may also have reduced energy needs. Therefore, future
321 work directly assessing mitochondrial function will help to discern between these
322 possibilities. Regardless, hibernation leads to a reduction in O_2 consumed in the
323 brainstem through altering the energy needs of different physiological processes.

324 We present three additional lines of evidence that neuronal activity incurs a lower
325 aerobic cost while maintaining normal function. In controls, activity declined with tissue
326 pO_2 and had a critical threshold where rhythmic output became disrupted. In contrast,
327 hibernators were stable from baseline to anoxia and lacked a measurable p_{crit}. This shows
328 that network function persists as aerobic metabolism decreases, and even ceases,
329 corroborating our previous reports[12,13]. Further supporting the reduced reliance on
330 aerobic respiration, increasing activity within the physiological range normally elevates O_2
331 consumption, but after hibernation, comparable increases in activity are met without
332 consuming further O_2. While the specific mechanisms for this are not yet known, we
333 hypothesize that glycolysis may be upregulated to provide ATP that supports the
334 increased demands of activity without supplying end-products to the mitochondria and/or
335 network efficiency increases to such a degree where enhanced activity requires minimal
336 additional ATP input. Finally, we demonstrate that disinhibition leads to substantial
337 oxygen consumption in both controls and hibernators, indicating that although the normal
338 dynamic range of activity is supported with less O_2 consumption, they retain a capacity to
339 increase aerobic metabolism during pathological hyperexcitability. Yet, following this
340 initial consumption event, hibernators stabilized at higher pO_2 values than controls while
341 maintaining normal activity. While reductions in GABA's contribution to rhythm generation
342 likely play a role[14], these results suggest that normal activity may be preserved because
343 of its reduced energetic requirements, improving the capacity to "share" energetic

resources with the elevated metabolic demands of seizure-like bursts. We present multiple lines of evidence that these circuits shift to consume less O_2, and we suggest that similar adaptations may extend to other species. For example, turtles and diving mammals and birds exhibit neural networks capable of maintaining function under low-oxygen conditions[47,48], suggesting that energy-efficient network function, as described here, may also apply to species traditionally viewed as hypoxia-tolerant. Overall, these results challenge the assumption that neuronal output is constrained by aerobic respiration, highlighting high-efficiency modes of neural communication as a plastic trait.

One additional intriguing feature of these results is that while activity consumed less O_2 across a range of intensities (Figure 1-3), hibernator mitochondria do not appear to be "dysfunctional" since they retain a capacity to aggressively consume O_2 during pathological hyperexcitability (Figure 4). This indicates the relationship between activity and O_2 operates with a reduced sensitivity, rather than being eliminated. The sensitivity of mitochondrial respiration to neural activity occurs through calcium-dependent mechanisms[49]. During presynaptic firing, calcium influx from extracellular sources enter mitochondria through mitochondrial calcium uniporter (MCU) to stimulate oxidative phosphorylation. MCU's high sensitivity for calcium uptake in neurons is controlled by a regulatory protein, mitochondrial calcium uptake 3 (MICU3), where its deletion reduces mitochondrial Ca^{2+} uptake and aerobic metabolism[6,50]. In contrast, MICU1 keeps MCU in a closed state, while MICU2 permits less calcium entry than MICU3, leading to less activity-dependent aerobic respiration[6,51,52]. While factors that control the calcium permeability of the MCU in our system are not known, it presents a biologically plausible explanation for alterations in the relationship between activity and O_2 consumption as we show: Hibernation may reduce mitochondrial calcium permeability, which prevents neural activity from increasing aerobic metabolism within the physiological range. However, after crossing a calcium threshold during pathological hyperexcitability, O_2 consumption accelerates. Future work should address the possibility of plasticity in coupling between activity and calcium-dependent activation of mitochondrial respiration.

CONCLUSION

Our findings reveal that neural circuits in the vertebrate brain can undergo a fundamental reorganization of the relationship between activity and O_2 consumption. By reducing the aerobic requirement for neural activity, the frog brainstem maintains stable network output under metabolic conditions that normally induce severe perturbations. A central element of this shift appears to be the enhanced efficiency of network function, which allows hibernators to generate normal output with less ongoing aerobic metabolism. These results raise questions about why most animals evolved, and default to, such energetically costly neural circuitry when more cost-effective solutions are physiologically possible and may already lie dormant in these very circuits. The ability to maintain functional network dynamics with less aerobic respiration is especially fascinating, as reductions in aerobic metabolism render many costly aspects of circuit function vulnerable in disorders such as Alzheimer's and Parkinson's disease[8]. By identifying mechanisms that allow circuits transition between states with vastly different aerobic demands needed to produce similar function, our work highlights how natural adaptation in diverse animal models can serve as valuable frameworks for exploring strategies to improve metabolic resilience in the mammalian brain.

Acknowledgements: The authors would like to thank Nik Bueschke and Jose Viteri for comments on the manuscript.

Figures and Legends

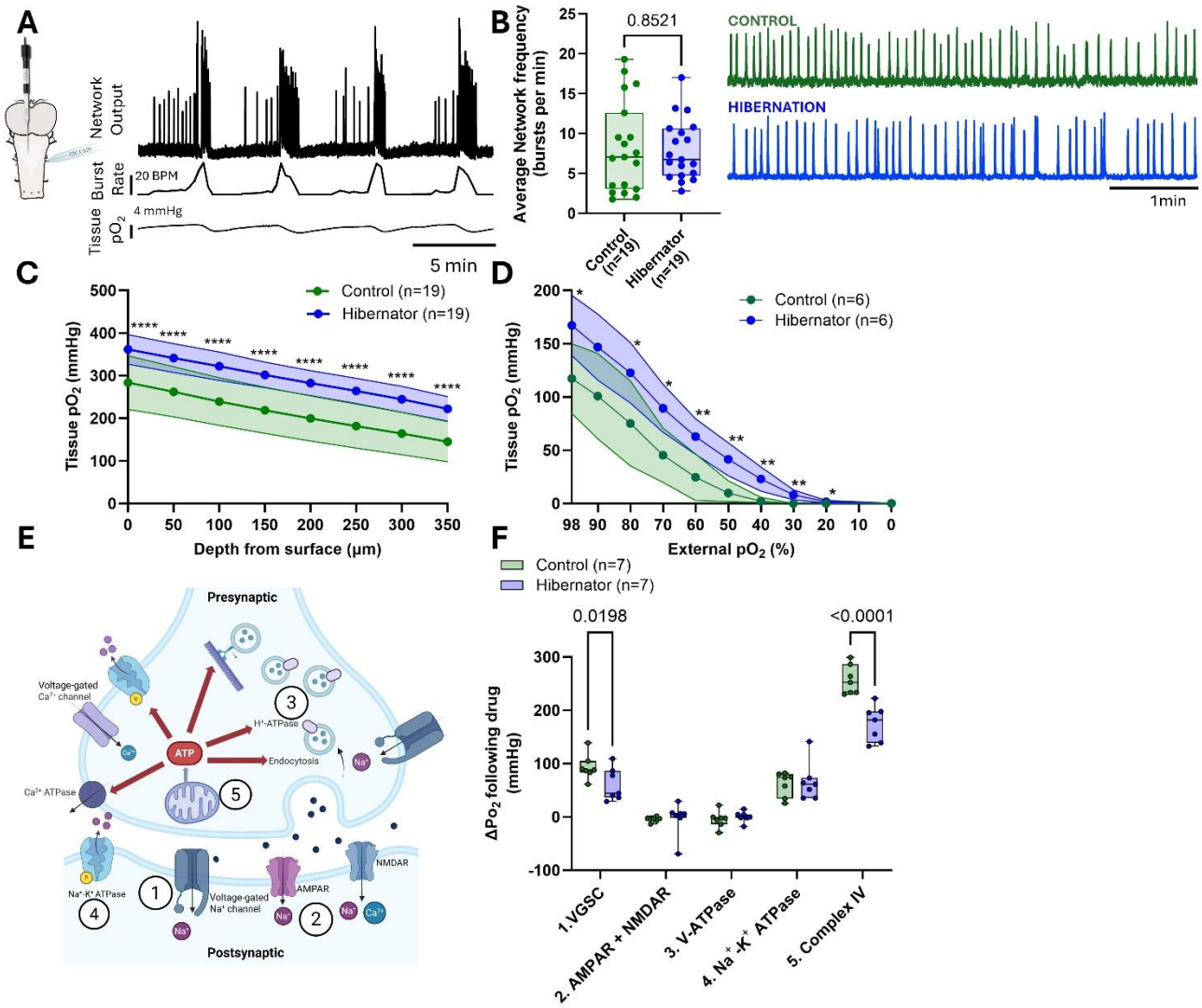

Figure 1. Hibernators have lower apparent oxygen consumption due to reduced energy demands of network activity and basal mitochondrial respiration.

A. Schematic of the brainstem preparation with an oxygen sensor placed in the proposed rhythm-generating region. Example recording shows synchronized vagus nerve activity, network frequency, and corresponding tissue pO_2 fluctuations.
B. Control and hibernator brainstems showed similar baseline burst frequency (unpaired t-test).

402 C. Tissue pO_2 depth profiles up to 350 μm showed significantly higher pO_2 in
403 hibernators (n = 19/group; repeated measures two-way ANOVA with Holm–Šidák
404 multiple comparisons test; ****$p < 0.0001$).
405 D. During gradual external pO_2 reduction, hibernator brainstems maintained higher
406 tissue pO_2 throughout hypoxia induction (n = 6/group; repeated measures two-way
407 ANOVA with Holm–Šidák multiple comparisons test; **$p<0.01$, *$p < 0.05$).
408 E. An illustration of major energy consuming pathways at the synapse with the
409 blocked pathways numbered (made in Biorender).
410 F. Summary of ΔpO_2 after blocking voltage-gated Na^+ channels, AMPA and NMDA
411 receptors, vesicular ATPase, Na^+-K^+ ATPase and mitochondrial Complex IV (n =
412 7/group). Hibernators showed significantly smaller ΔpO_2 with TTX and sodium
413 cyanide (two-way ANOVA with Holm–Šidák multiple comparisons test).

414

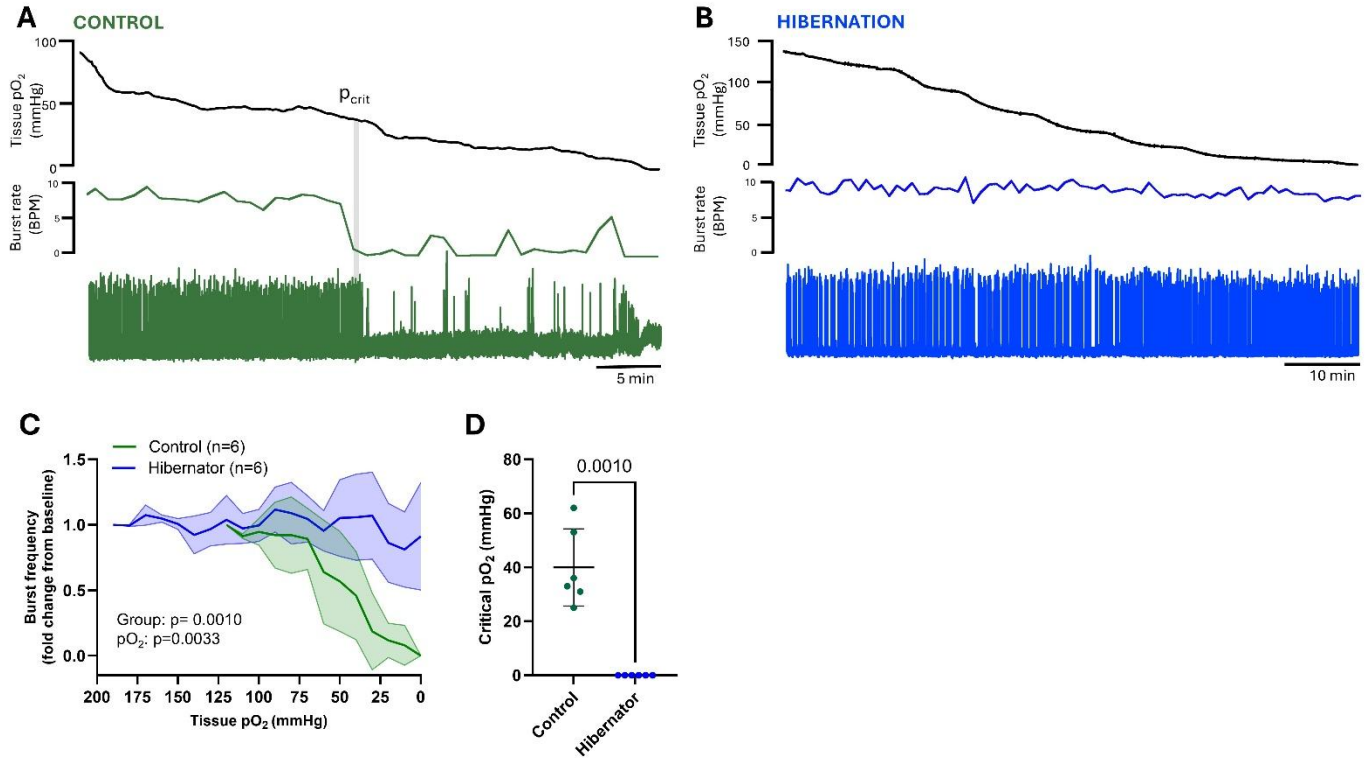

Figure 2. Brainstem motor activity no longer requires aerobic respiration after hibernation

A. Example of graded hypoxia experiment in a control, where nerve burst frequency declined strongly at a critical threshold (p_{crit}).
B. In hibernators (n = 6), neural activity remained stable even as tissue pO_2 at ~0 mmHg.
C. Mean ± SD of fold change in burst frequency are shown for control and hibernator (n = 6 each) groups. Controls show a lower starting pO_2 with an inflection point and subsequent decline in burst frequency as pO_2 decreases, whereas hibernators have higher starting pO_2 and remain relatively stable across the pO_2 range. P values of group and pO_2 from linear mixed model are shown in the figure.
D. Critical pO_2 thresholds: controls lost rhythmic activity at significantly higher pO_2 than hibernators, which showed no apparent critical pO_2 threshold as all preparations were active at 0 mmHg, and therefore assigned a p_{crit} value of 0 mmHg (p = 0.001, unpaired t-test).

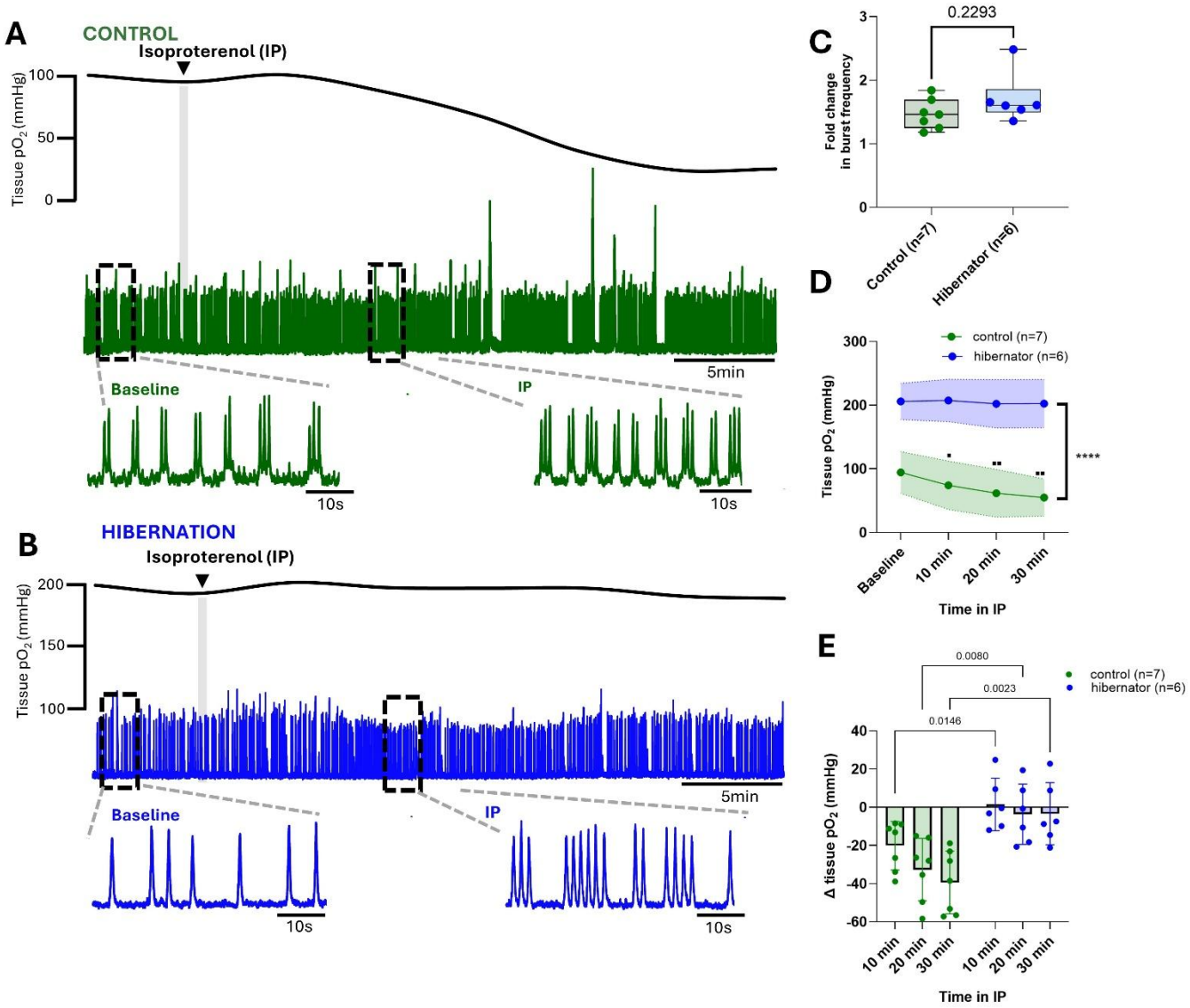

Figure 3. Hibernators sustain elevated neural activity without consuming more oxygen.

A. Representative traces showing changes in tissue pO_2 and vagus nerve activity during isoproterenol exposure in a control brainstem. Increased burst frequency caused a drop in tissue pO_2. The insets show nerve activity of control brainstem at baseline and during isoproterenol exposure.

B. Tissue pO_2 in hibernators remained stable during elevated burst frequency. The insets show nerve activity of hibernator brainstem at baseline and during isoproterenol exposure.

C. Fold change in burst frequency during isoproterenol application for controls (n=7) and hibernators (n=6; unpaired t test). Two-tailed unpaired t test.

D. Absolute tissue pO_2 at different timepoints of isoproterenol application show a significant drop from baseline tissue pO_2 in the controls but no change in hibernators. **** indicates $p<0.0001$ between controls and hibernators at all time points, and ■■$p<0.01$, and ■ $p<0.05$ indicate differences from baseline within the control group from Holm-Sidak Multiple Comparisons tests following repeated measures two-way ANOVA.

E. ΔpO_2 at 10, 20, and 30 minutes of isoproterenol application for controls and hibernators (repeated measures two-way ANOVA followed by Holm–Šidák multiple comparisons test).

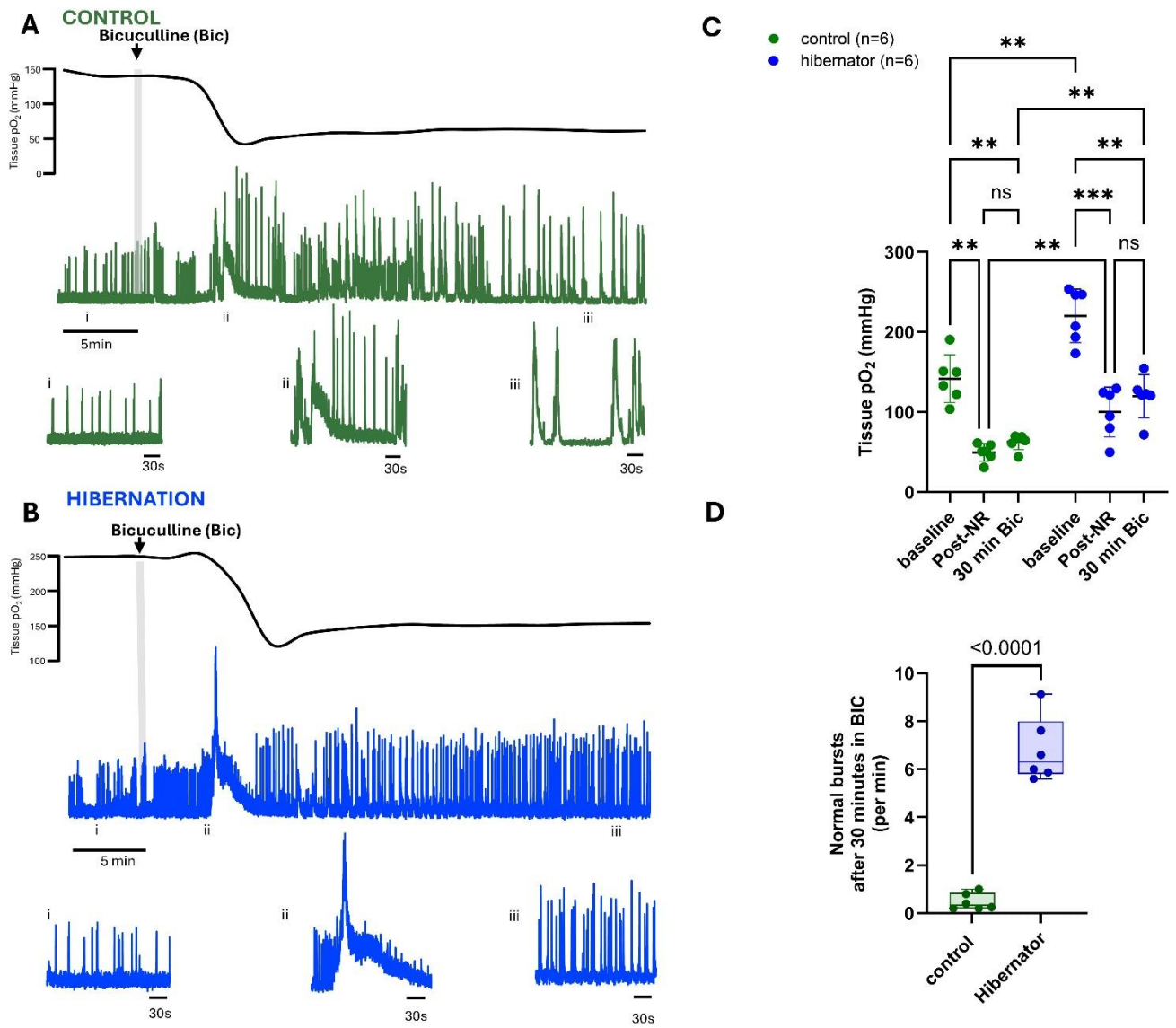

Figure 4. Hibernators rely on aerobic metabolism during pathological hyperexcitability but maintain elevated tissue oxygen.

A. Representative recordings of tissue pO_2 and vagus nerve activity in a control brainstem during application of the $GABA_A$ receptor antagonist, bicuculline. Expanded nerve traces show baseline respiratory activity (RESP), the first large chaotic burst during bicuculline application, and then at the end of the 30 minute bicuculline exposure.

B. Representative recordings of tissue pO_2 and nerve activity in a hibernator brainstem during application of bicuculline. Expanded nerve traces show baseline

461 respiratory activity (RESP), the first large chaotic burst during bicuculline
462 application, and then at the end of the 30-minute bicuculline exposure.
463 C. Absolute tissue pO_2 at baseline, immediately after the first major non-respiratory
464 burst (post-NR), and at the end of bicuculline treatment in control and hibernator
465 brainstems. Both controls and hibernators face a significant drop in tissue pO_2
466 post-NR, however tissue pO_2 settles at a higher level in hibernators as compared
467 to controls (n=6 per group; repeated two-way ANOVA followed by Holm-Šídák's
468 multiple comparisons test, ***$p<0.001$, **$p<0.01$).
469 D. Number of normal bursts per minute after 30 minutes of bicuculline application in
470 control and hibernator brainstem (n=6 per group; unpaired t test).

471 **References**

472 1. Attwell, D., and Laughlin, S.B. (2001). An Energy Budget for Signaling in the Grey
473 Matter of the Brain. Journal of Cerebral Blood Flow & Metabolism *21*, 1133–1145.
474 https://doi.org/10.1097/00004647-200110000-00001.

475 2. Niven, J.E., and Laughlin, S.B. (2008). Energy limitation as a selective pressure
476 on the evolution of sensory systems. Journal of Experimental Biology *211*, 1792–
477 1804. https://doi.org/10.1242/jeb.017574.

478 3. Trevisiol, A., Saab, A.S., Winkler, U., Marx, G., Imamura, H., Möbius, W., Kusch,
479 K., Nave, K.-A., and Hirrlinger, J. (2017). Monitoring ATP dynamics in electrically active
480 white matter tracts. Elife *6*. https://doi.org/10.7554/eLife.24241.

481 4. Hall, C.N., Klein-Flugge, M.C., Howarth, C., and Attwell, D. (2012). Oxidative
482 Phosphorylation, Not Glycolysis, Powers Presynaptic and Postsynaptic Mechanisms
483 Underlying Brain Information Processing. Journal of Neuroscience *32*, 8940–8951.
484 https://doi.org/10.1523/JNEUROSCI.0026-12.2012.

485 5. Özugur, S., Kunz, L., and Straka, H. (2020). Relationship between oxygen
486 consumption and neuronal activity in a defined neural circuit. BMC Biol. *18*, 76.
487 https://doi.org/10.1186/s12915-020-00811-6.

488 6. Ashrafi, G., de Juan-Sanz, J., Farrell, R.J., and Ryan, T.A. (2020). Molecular
489 Tuning of the Axonal Mitochondrial Ca2+ Uniporter Ensures Metabolic Flexibility of
490 Neurotransmission. Neuron *105*, 678-687.e5.
491 https://doi.org/10.1016/j.neuron.2019.11.020.

492 7. Rangaraju, V., Calloway, N., and Ryan, T.A. (2014). Activity-Driven Local ATP
493 Synthesis Is Required for Synaptic Function. Cell *156*, 825–835.
494 https://doi.org/10.1016/j.cell.2013.12.042.

495 8. Li, S., and Sheng, Z.-H. (2022). Energy matters: presynaptic metabolism and the
496 maintenance of synaptic transmission. Nat. Rev. Neurosci. *23*, 4–22.
497 https://doi.org/10.1038/s41583-021-00535-8.

498 9. Chklovskii, D.B., Schikorski, T., and Stevens, C.F. (2002). Wiring Optimization in
499 Cortical Circuits. Neuron *34*, 341–347. https://doi.org/10.1016/S0896-
500 6273(02)00679-7.

501 10. Adams, S., Zubov, T., Bueschke, N., and Santin, J.M. (2021). Neuromodulation
502 or energy failure? Metabolic limitations silence network output in the hypoxic amphibian
503 brainstem. Am. J. Physiol. Regul. Integr. Comp. Physiol. *320*, R105–R115.
504 https://doi.org/10.1152/AJPREGU.00209.2020.

505 11. Winmill, R.E., Chen, A.K., and Hedrick, M.S. (2005). Development of the
506 respiratory response to hypoxia in the isolated brainstem of the bullfrog Rana
507 catesbeiana. Journal of experimental biology *208*, 213–222.
508 https://doi.org/10.1242/jeb.01399.

509 12. Bueschke, N., Do Amaral-Silva, L., Adams, S., and Santin, J.M. (2021).
510 Transforming a neural circuit to function without oxygen and glucose delivery. Current
511 Biology *31*, R1564–R1565. https://doi.org/10.1016/j.

512 13. Amaral-Silva, L., and Santin, J.M. (2023). Synaptic modifications transform
513 neural networks to function without oxygen. BMC Biol. *21*, 54.
514 https://doi.org/10.1186/s12915-023-01518-0.

515 14. Saunders, S.E., and Santin, J.M. (2024). Hibernation reduces GABA signaling in
516 the brainstem to enhance motor activity of breathing at cool temperatures. BMC
517 Biol. *22*, 251. https://doi.org/10.1186/s12915-024-02050-5.

518 15. Kottick, A., Baghdadwala, M.I., Ferguson, E. V., and Wilson, R.J.A. (2013).
519 Transmission of the respiratory rhythm to trigeminal and hypoglossal motor neurons in
520 the American Bullfrog (Lithobates catesbeiana). Respir. Physiol. Neurobiol. *188*, 180–
521 191. https://doi.org/10.1016/j.resp.2013.06.008.

522 16. Chen, A.K., and Hedrick, M.S. (2008). Role of glutamate and substance P in the
523 amphibian respiratory network during development. Respir. Physiol. Neurobiol. *162*, 24–
524 31. https://doi.org/10.1016/j.resp.2008.03.010.

525 17. Hardie, D.G. (2000). Metabolic control: A new solution to an old problem. Current
526 Biology *10*, R757–R759. https://doi.org/10.1016/S0960-9822(00)00744-2.

527 18. Sengupta, B., Stemmler, M., Laughlin, S.B., and Niven, J.E. (2010). Action
528 Potential Energy Efficiency Varies Among Neuron Types in Vertebrates and
529 Invertebrates. PLoS Comput. Biol. *6*, e1000840.
530 https://doi.org/10.1371/journal.pcbi.1000840.

531 19. Harris, J.J., Jolivet, R., Engl, E., and Attwell, D. (2015). Energy-Efficient
532 Information Transfer by Visual Pathway Synapses. Current Biology *25*, 3151–
533 3160. https://doi.org/10.1016/j.cub.2015.10.063.

534 20. Alle, H., Roth, A., and Geiger, J.R.P. (2009). Energy-Efficient Action Potentials in
535 Hippocampal Mossy Fibers. Science (1979). *325*, 1405–1408.
536 https://doi.org/10.1126/science.1174331.

537 21. Bueschke, N., Amaral-Silva, L., Hu, M., Alvarez, A., and Santin, J.M. (2024).
538 Plasticity in the Functional Properties of NMDA Receptors Improves Network

539 Stability during Severe Energy Stress. Journal of Endocrinology *44*, 1–12.
540 https://doi.org/10.1523/JNEUROSCI.0502-23.2024.

541 22. Harris, J.J., and Attwell, D. (2012). The Energetics of CNS White Matter. The
542 Journal of Neuroscience *32*, 356–371. https://doi.org/10.1523/JNEUROSCI.3430-
543 11.2012.

544 23. Donohoe, P.H., West, T.G., and Boutilier, R.G. (1998). Respiratory, metabolic,
545 and acid-base correlates of aerobic metabolic rate reduction in overwintering frogs.
546 American Journal of Physiology-Regulatory, Integrative and Comparative Physiology
547 *274*, R704–R710. https://doi.org/10.1152/ajpregu.1998.274.3.R704.

548 24. Burton, M.T., and Santin, J.M. (2020). A direct excitatory action of lactate ions in
549 the central respiratory network of bullfrogs, Lithobates catesbeianus. Journal of
550 Experimental Biology *223*, jeb235705. https://doi.org/10.1242/jeb.235705.

551 25. Oku, Y., Kimura, N., Masumiya, H., and Okada, Y. (2008). Spatiotemporal
552 organization of frog respiratory neurons visualized on the ventral medullary
553 surface. Respir. Physiol. Neurobiol. *161*, 281–290.
554 https://doi.org/10.1016/j.resp.2008.03.002.

555 26. Reid, S.G., and Milsom, W.K. (1998). Respiratory pattern formation in the isolated
556 bullfrog (Rana catesbeiana) brainstem-spinal cord. Respir. Physiol. *114*, 239–255.
557 https://doi.org/10.1016/S0034-5687(98)00091-7.

558 27. Lecoq, J., Tiret, P., Najac, M., Shepherd, G.M., Greer, C.A., and Charpak, S.
559 (2009). Odor-Evoked Oxygen Consumption by Action Potential and Synaptic
560 Transmission in the Olfactory Bulb. The Journal of Neuroscience *29*, 1424–1433.
561 https://doi.org/10.1523/JNEUROSCI.4817-08.2009.

562 28. Broch, L., Morales, R., Sandoval, A., and Hedrick, M. (2002). Regulation of the
563 respiratory central pattern generator by chloride-dependent inhibition during
564 development in the bullfrog (Rana catesbeiana). Journal of Experimental Biology
565 *205*, 1161–1169. https://doi.org/10.1242/jeb.205.8.1161.

566 29. Kogo, N., Perry, S.F., and Remmers, J.E. (1994). Neural organization of the
567 ventilatory activity in the frog, Rana catesbeiana. J. Neurobiol. *25*, 1067–1079.
568 https://doi.org/10.1002/neu.480250904.

569 30. Milsom, W.K., Reid, S.G., Meier, J.T., and Kinkead, R. (1999). Central respiratory
570 pattern generation in the bullfrog, Rana catesbeiana. Comparative Biochemistry
571 and Physiology Part A *124*, 253–264. https://doi.org/10.1016/S1095-
572 6433(99)00113-0.

573 31. Pulido, C., and Ryan, T.A. (2021). Synaptic vesicle pools are a major hidden
574 resting metabolic burden of nerve terminals. Sci. Adv. *7*.
575 https://doi.org/10.1126/sciadv.abi9027.

576 32. Cannon, D.J., and Santin, J.M. (2025). Homeostatic regulation of a motor circuit
577 through temperature sensing rather than activity sensing. Current Biology *35*,
578 2256-2265.e3. https://doi.org/10.1016/j.cub.2025.03.054.

579 33. Justs, K.A., Lu, Z., Chouhan, A.K., Borycz, J.A., Lu, Z., Meinertzhagen, I.A., and
580 Macleod, G.T. (2022). Presynaptic Mitochondrial Volume and Packing Density
581 Scale with Presynaptic Power Demand. The Journal of Neuroscience *42*, 954–
582 967. https://doi.org/10.1523/JNEUROSCI.1236-21.2021.

583 34. Meir, J.U., Champagne, C.D., Costa, D.P., Williams, C.L., and Ponganis, P.J.
584 (2009). Extreme hypoxemic tolerance and blood oxygen depletion in diving
585 elephant seals. Am J Physiol Regul Integr Comp Physiol *297*, 927–939.
586 https://doi.org/10.1152/ajpregu.00247.2009.-Species.

587 35. Buck, L.T., and Pamenter, M.E. (2018). The hypoxia-tolerant vertebrate brain:
588 Arresting synaptic activity. Comp. Biochem. Physiol. B Biochem. Mol. Biol. *224*, 61–70.
589 https://doi.org/10.1016/j.cbpb.2017.11.015.

590 36. Amaral-Silva, L., and Santin, J. (2024). Neural Processing without O2 and
591 Glucose Delivery: Lessons from the Pond to the Clinic. Physiology *39*, 360–372.
592 https://doi.org/10.1152/physiol.00030.2023.

593 37. Cunnane, S.C., Trushina, E., Morland, C., Prigione, A., Casadesus, G., Andrews,
594 Z.B., Beal, M.F., Bergersen, L.H., Brinton, R.D., de la Monte, S., et al. (2020).
595 Brain energy rescue: an emerging therapeutic concept for neurodegenerative
596 disorders of ageing. Nat. Rev. Drug Discov. *19*, 609–633.
597 https://doi.org/10.1038/s41573-020-0072-x.

598 38. Larson, J., Drew, K.L., Folkow, L.P., Milton, S.L., and Park, T.J. (2014). No
599 oxygen? No problem! intrinsic brain tolerance to hypoxia in vertebrates. Journal of
600 Experimental Biology *217*, 1024–1039. https://doi.org/10.1242/jeb.085381.

601 39. Harris, J.J., Jolivet, R., and Attwell, D. (2012). Synaptic Energy Use and Supply.
602 Neuron *75*, 762–777. https://doi.org/10.1016/j.neuron.2012.08.019.

603 40. Howarth, C., Gleeson, P., and Attwell, D. (2012). Updated Energy Budgets for
604 Neural Computation in the Neocortex and Cerebellum. Journal of Cerebral Blood
605 Flow & Metabolism *32*, 1222–1232. https://doi.org/10.1038/jcbfm.2012.35.

606 41. Ballinger, M.A., Schwartz, C., and Andrews, M.T. (2017). Enhanced oxidative
607 capacity of ground squirrel brain mitochondria during hibernation. J Physiol Regul Integr
608 Comp Physiol *312*, 301–310. https://doi.org/10.1152/ajpregu.00314.2016.-Dur.

609 42. Salin, K., Auer, S.K., Rey, B., Selman, C., and Metcalfe, N.B. (2015). Variation in
610 the link between oxygen consumption and ATP production, and its relevance for animal
611 performance. Proceedings of the Royal Society B: Biological Sciences *282*, 20151028.
612 https://doi.org/10.1098/rspb.2015.1028.

613 43. Divakaruni, A.S., and Brand, M.D. (2011). The Regulation and Physiology of
614 Mitochondrial Proton Leak. Physiology *26*, 192–205.
615 https://doi.org/10.1152/physiol.00046.2010.

616 44. Hoang, T., Kuljanin, M., Smith, M.D., and Jelokhani-Niaraki, M. (2015). A
617 biophysical study on molecular physiology of the uncoupling proteins of the
618 central nervous system. Biosci. Rep. *35*, e00226.
619 https://doi.org/10.1042/BSR20150130.

620 45. Decker, S.T., and Funai, K. (2024). Mitochondrial membrane lipids in the
621 regulation of bioenergetic flux. Cell Metab. *36*, 1963–1978.
622 https://doi.org/10.1016/j.cmet.2024.07.024.

623 46. Engl, E., and Attwell, D. (2015). Non-signalling energy use in the brain. J. Physiol.
624 *593*, 3417–3429. https://doi.org/10.1113/jphysiol.2014.282517.

625 47. Ramirez, J.-M., Folkow, L.P., and Blix, A.S. (2007). Hypoxia Tolerance in
626 Mammals and Birds: From the Wilderness to the Clinic. Annu. Rev. Physiol. *69*,
627 113–143. https://doi.org/10.1146/annurev.physiol.69.031905.163111.

628 48. Ariel, M., Ahuja, S., and Warren, D.E. (2023). Responses of the in vitro turtle brain
629 to visual and auditory stimuli during severe hypoxia. Journal of Experimental
630 Biology *226*, jeb244687. https://doi.org/10.1242/jeb.244687.

631 49. Hayakawa, Y., Nemoto, T., Iino, M., and Kasai, H. (2005). Rapid Ca2+-dependent
632 increase in oxygen consumption by mitochondria in single mammalian central
633 neurons. Cell Calcium *37*, 359–370. https://doi.org/10.1016/j.ceca.2004.11.005.

634 50. Patron, M., Granatiero, V., Espino, J., Rizzuto, R., and De Stefani, D. (2019).
635 MICU3 is a tissue-specific enhancer of mitochondrial calcium uptake. Cell Death
636 Differ. *26*, 179–195. https://doi.org/10.1038/s41418-018-0113-8.

637 51. Mallilankaraman, K., Doonan, P., Cárdenas, C., Chandramoorthy, H.C., Müller,
638 M., Miller, R., Hoffman, N.E., Gandhirajan, R.K., Molgó, J., Birnbaum, M.J., et al.
639 (2012). MICU1 Is an Essential Gatekeeper for MCU-Mediated Mitochondrial Ca2+

640 Uptake that Regulates Cell Survival. Cell *151*, 630–644.
641 https://doi.org/10.1016/j.cell.2012.10.011.

642 52. Patron, M., Checchetto, V., Raffaello, A., Teardo, E., Vecellio Reane, D.,
643 Mantoan, M., Granatiero, V., Szabò, I., De Stefani, D., and Rizzuto, R. (2014). MICU1
644 and MICU2 Finely Tune the Mitochondrial Ca2+ Uniporter by Exerting Opposite Effects
645 on MCU Activity. Mol. Cell *53*, 726–737. https://doi.org/10.1016/j.molcel.2014.01.013.

646